

Capturing reaction paths and intermediates in Cre-loxP recombination using single-molecule fluorescence

Justin N. M. Pinkney^{a,1}, Paweł Zawadzki^{b,1}, Jarosław Mazuryk^{c,d}, Lidia K. Arciszewska^b, David J. Sherratt^b, and Achillefs N. Kapanidis^{a,2}

^aBiological Physics Research Group, Clarendon Laboratory, Department of Physics, University of Oxford, Oxford OX1 3PU, United Kingdom; ^bDepartment of Biochemistry, University of Oxford, Oxford OX1 3QU, United Kingdom; ^cNanobiomedical Centre, A. Mickiewicz University, 61-614 Poznań, Poland; and ^dMolecular Biophysics Division, Faculty of Physics, A. Mickiewicz University, 61-614 Poznań, Poland

Edited by Arthur Landy, Brown University, Providence, RI, and approved October 15, 2012 (received for review July 19, 2012)

Site-specific recombination plays key roles in microbe biology and is exploited extensively to manipulate the genomes of higher organisms. Cre is a well studied site-specific recombinase, responsible for establishment and maintenance of the P1 bacteriophage genome in bacteria. During recombination, Cre forms a synaptic complex between two 34-bp DNA sequences called *loxP* after which a pair of strand exchanges forms a Holliday junction (HJ) intermediate; HJ isomerization then allows a second pair of strand exchanges and thus formation of the final recombinant product. Despite extensive work on the Cre-*loxP* system, many of its mechanisms have remained unclear, mainly due to the transient nature of complexes formed and the ensemble averaging inherent to most biochemical work. Here, we address these limitations by introducing tethered fluorophore motion (TFM), a method that monitors large-scale DNA motions through reports of the diffusional freedom of a single fluorophore. We combine TFM with Förster resonance energy transfer (FRET) and simultaneously observe both large- and small-scale conformational changes within single DNA molecules. Using TFM-FRET, we observed individual recombination reactions in real time and analyzed their kinetics. Recombination was initiated predominantly by exchange of the “bottom-strands” of the DNA substrate. In productive complexes we used FRET distributions to infer rapid isomerization of the HJ intermediates and that a rate-limiting step occurs after this isomerization. We also observed two nonproductive synaptic complexes, one of which was structurally distinct from conformations in crystals. After recombination, the product synaptic complex was extremely stable and refractory to subsequent rounds of recombination.

tethered fluorophore motion | site-specific DNA recombination | Holliday junction dynamics | alternating laser excitation | protein-DNA interactions

Site-specific DNA recombination is the protein-mediated cleavage, exchange, and rejoicing of DNA strands between two duplexes containing a specific sequence. Tyrosine recombinases are involved in the integration and excision of viral genomes, resolution of chromosome dimers, and gene expression (1). This large family of proteins shares a general mechanism of recombination whereby a tetramer of recombinases mediates sequential pairs of strand exchange between two DNA duplexes; the first pair forms a Holliday junction (HJ) intermediate, whereas the second leads to resolution of the HJ to recombinant product (Fig. 1A). DNA cleavage requires no external energy factors, as the bond energy is stored during strand exchange as a covalent protein-DNA linkage.

One of the best studied tyrosine recombinases is Cre, a 38 kDa protein of the bacteriophage P1 of *Escherichia coli*. Cre catalyzes cyclization of the viral genome and resolution of plasmid dimers during replication (2). Cre mediates recombination between 34 bp DNA sequences named *loxP* (Fig. 1B). Unlike other recombinases [e.g., XerCD (3) and λ Int (4)], Cre does not require accessory proteins and has been well studied genetically, biochemically, and structurally; consequently, it serves as an excellent model system for understanding the mechanisms of tyrosine recombinases. Its simplicity and compatibility with eukaryotes has also made it a

versatile tool for rearrangement and manipulation of genetic elements *in vivo* (5).

Structural studies on Cre-*loxP* reaction intermediates have identified nucleoprotein complexes with remarkably similar overall structure (near-square planar) at each stage of recombination. This structure involves four Cre monomers, bound to two anti-parallel *loxP* sites (Fig. 1) connected through a network of protein–protein interactions; of these four monomers, only two are active at any time (Fig. 1A, green monomers). After the first pair of strand exchanges, only subtle structural changes are needed to activate the second pair of Cre monomers. It is widely believed that all steps of recombination occur within this nucleoprotein complex without major changes to its architecture (2).

There is strong structural and biochemical evidence that Cre cleaves and exchanges DNA strands in an ordered fashion, with most studies finding recombination to be initiated with the “bottom-strands” (BSs) exchanged first (Fig. 1A and B, black DNA) (6–8). However, many of these studies relied on mutations in either Cre or *loxP*, and there are conflicting reports on the order of strand exchange (9, 10).

Characterizing short-lived species using ensemble biochemical techniques and relating them directly to the progress of reactions is challenging. To overcome complications caused by ensemble averaging and observe site-specific recombination in real time, various single-molecule techniques have been used, including atomic force microscopy (11), tethered particle motion (TPM) (4, 12), and magnetic tweezers (13). In particular, the recent TPM work by Fan et al. (12) observed the overall progress of recombination reactions, measuring various association and dissociation rates as well as noting the heterogeneous behavior of complexes, but was unable to correlate these changes to nanometer-scale rearrangements within individual complexes.

To address such limitations, we introduce tethered fluorophore motion (TFM), a method that monitors large-scale DNA motions through reports of the diffusional freedom of a fluorophore attached to DNA. We use alternating-laser excitation (ALEX) (14) to combine TFM with Förster resonance energy transfer (FRET) and simultaneously observe both large- and small-scale conformational changes of single DNA molecules. Using TFM-FRET, we observed recombination within individual nucleoprotein complexes in real time and analyzed their reaction kinetics. Our results showed that recombination is initiated predominantly by

Author contributions: J.N.M.P., P.Z., L.K.A., D.J.S., and A.N.K. designed research; J.N.M.P., P.Z., and J.M. performed research; J.N.M.P. and P.Z. analyzed data; and J.N.M.P., P.Z., L.K.A., D.J.S., and A.N.K. wrote the paper.

The authors declare no conflict of interest.

This article is a PNAS Direct Submission.

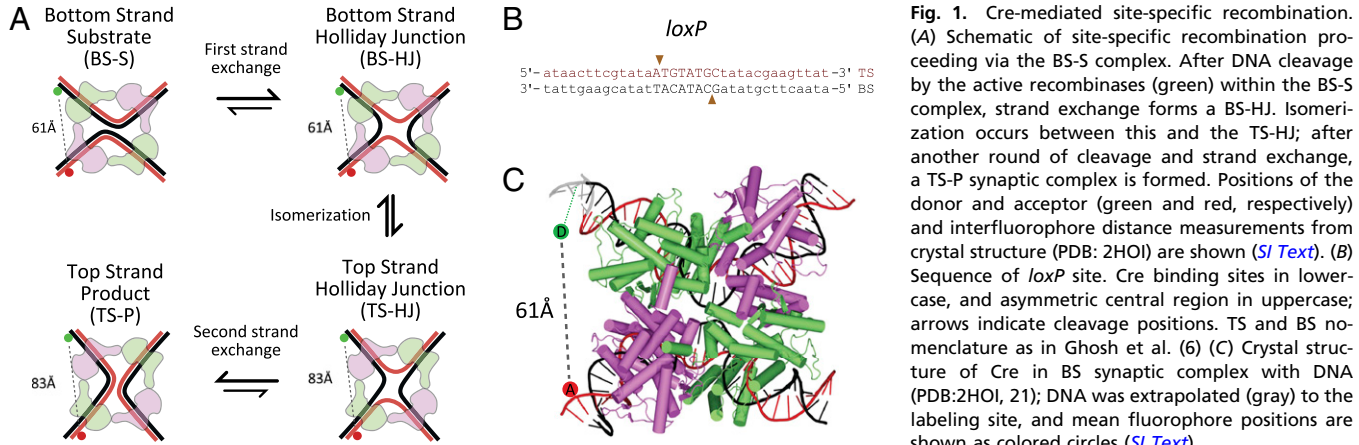
Freely available online through the PNAS open access option.

See Commentary on page 20779.

¹J.N.M.P. and P.Z. contributed equally to this work.

²To whom correspondence should be addressed. E-mail: a.kapanidis1@physics.ox.ac.uk.

This article contains supporting information online at www.pnas.org/lookup/suppl/doi:10.1073/pnas.1211922109/-DCSupplemental.



exchange of the BSs rather than the “top-strands” (TSs) and that synaptic complex formation is reversible. In productive complexes, we identified a rate-limiting step that occurs after HJ isomerization. We also observed two nonproductive synaptic complexes, one of which was structurally distinct from the conformations seen in crystals. Finally, we were able to infer fast HJ dynamics in recombining complexes and demonstrate the slow dissociation of the recombined product synaptic complex.

Results

Monitoring Recombination in Real Time Within Single Cre-*loxP* Complexes.

To observe recombination at the single-molecule level, we use TFM for monitoring large-scale conformational changes in DNA and combine it with the single-molecule FRET capability of ALEX for simultaneous monitoring of nanoscale changes. In our study, we prepared 1,087-bp-long DNA substrates (containing two *loxP* sites; *SI Text* and Fig. S1) labeled with a FRET donor and acceptor, tethered them to a PEG-passivated glass coverslip (Fig. 2A) using a biotin–neutravidin interaction (15), and observed them using total-internal reflection fluorescence (TIRF) microscopy. Because the fluorophores were attached at either end of the DNA substrate, the interfluorophore distance was well beyond the range of FRET.

Cre-mediated formation of a synaptic complex between the *loxP* sites dramatically reduced the interfluorophore distance (Fig. 2A, yellow panel). Donor and acceptor fluorophores were positioned such that formation of a Cre-*loxP* antiparallel synapsis [with the BSs in an active conformation for cleavage; Fig. 1A, BS synaptic (BS-S) complex] resulted in a significant FRET signal (apparent FRET efficiency, $E^* > 0.2$). Parallel Cre-*loxP* synaptic complexes, which are known to assemble but not recombine (2), were not expected to show significant FRET and were not addressed in this work. Due to structural similarities of the BS-S complex and the BS-HJ (Figs. 1A and 2A), the FRET efficiency of these two states is expected to be identical. Any complexes following HJ isomerization [TS-HJ, TS product (TS-P) synaptic complex, and the product DNA], were expected to show low FRET ($E^* < 0.2$; Fig. 2A, pink panels; *SI Text*). Consequently, the FRET efficiency could not distinguish directly between complexes that isomerize to a TS complex (TS-HJ or TS-P) and complexes that dissociate back to the substrate DNA.

To discriminate between the above possibilities, we developed TFM (in analogy to TPM) to probe the diffusional freedom of the surface-distal DNA end. As the 1,087 bp substrate is much longer than the persistence length of DNA (~150 bp; ~50 nm), the surface-distal end (and thus the attached fluorophore) is free to diffuse above the surface and around the tether point. Because this motion occurs at the millisecond timescale (16), each image of the surface-distal fluorophore represented the average position of the

DNA end during the camera exposure time (100 ms). We thus expected an attenuated fluorescence emission from the fluorophore as its average position is significantly above the surface, where the excitation power is reduced due to the exponential decay of the evanescent wave generated in TIRF (17). Further, due to in-plane motion of the DNA above the surface, we expected that the surface-distal fluorophore would yield a point-spread-function (PSF) wider than the diffraction-limited PSF (~150 nm) observed for immobilized fluorophores with a short (1–10 nm) tether. Combining the observables of TFM and FRET allowed us to directly monitor reaction intermediates during recombination.

To assess the efficiency of recombination on the surface, we incubated coverslips carrying immobilized 1,087-bp-long DNA substrate (BS FRET; Fig. S1) with Cre for 10 min. After washing the surface with SDS to disrupt protein interactions, we identified DNA molecules that had undergone recombination; such molecules were expected to be short (61 bp), be doubly labeled, and have a surface-proximal acceptor (i.e., a diffraction-limited PSF). Indeed, ~30% of the molecules showed a PSF width corresponding to a surface-proximal fluorophore (Fig. S2), indicating that many molecules had undergone at least one pair of strand exchanges; this percentage is comparable to reactions performed in solution (Fig. S3) (18).

To monitor individual recombination reactions in real time, we acquired several 100-s movies during incubation of Cre with the surface-immobilized BS FRET substrate. We detected transient FRET signals (dwells with $E^* > 0.2$; *SI Text*) from 178 of 6,548 observed DNA molecules (Fig. 2, yellow panels). The transient FRET signals were concurrent with a decrease in acceptor PSF width and were consistent with BS complex formation. The number of analyzed events was limited by the restricted observation time (due to photobleaching) and by complex photophysics of some fluorophores; however, we estimate a probability of BS complex formation per particle of $P \approx 3.8 \times 10^{-4} \text{ s}^{-1}$ (*SI Text*).

We then classified molecules undergoing BS complex formation according to the PSF width after loss of the transient FRET signal. The majority of molecules (76%) showed a PSF that remained narrow after the decrease in FRET, representing complexes that progressed through HJ isomerization, reaching either a TS complex (TS-HJ or TS-P) or dissociated recombinant product (Fig. 2A, pink panels). Previous studies have shown that Cre-*loxP* TS-HJs are efficiently resolved to recombinant product (19); we thus believe that the majority of complexes after HJ isomerization have undergone two pairs of strand exchange and formed a recombinant product, and we classify them as “productive complexes.” The remainder of molecules, where the PSF returns to that of free substrate DNA (Fig. 3B, left panel), represented BS complexes that dissociated back to the substrate (either having formed a BS-HJ intermediate or not), and we classify them as “nonproductive complexes.”

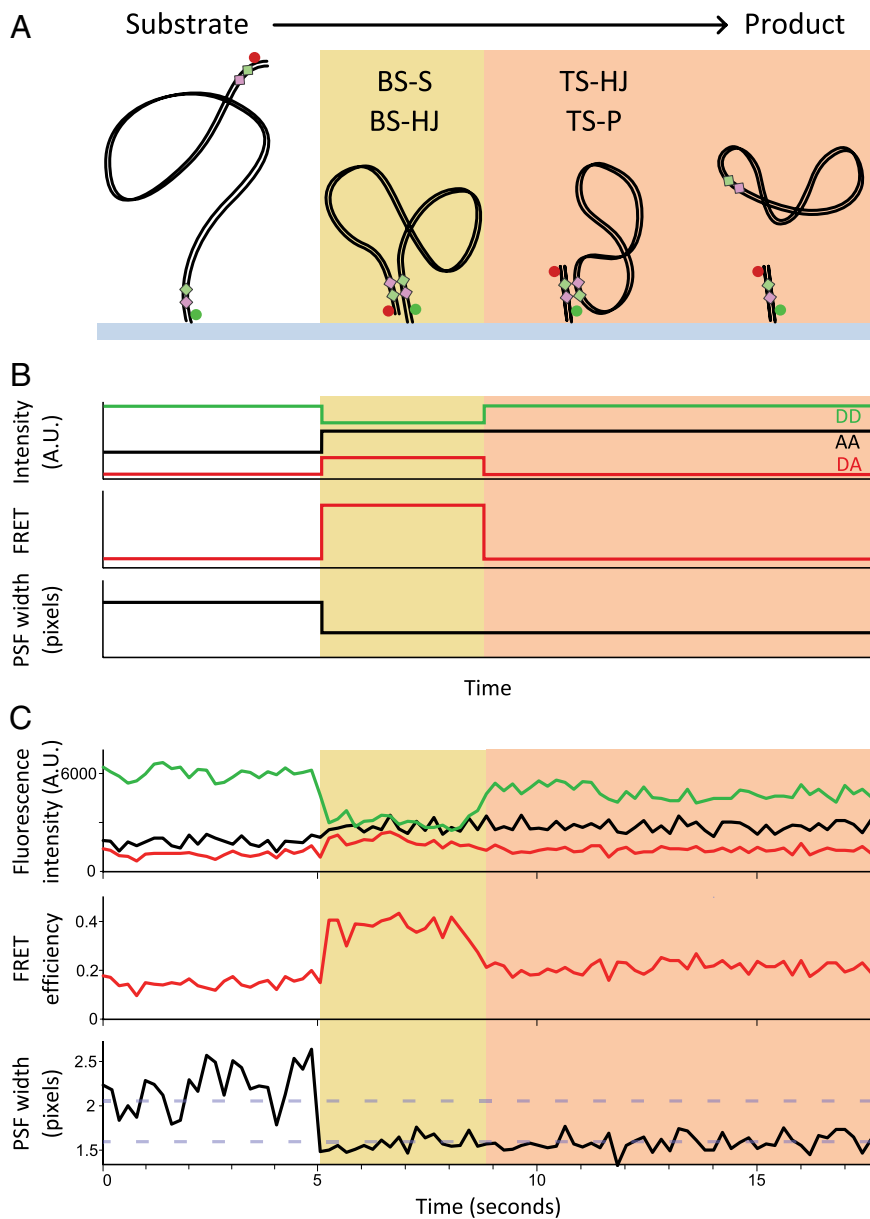


Fig. 2. Single-molecule recombination observed in real time. (A) Schematic of BS FRET substrate during BS recombination. (B) Expected emission intensities of donor (DD, green) and acceptor under green excitation (DA, red) and acceptor under red excitation (AA, black). DD and DA are used to calculate apparent FRET efficiency (E^*), and the PSF width of the acceptor is obtained from AA images. The stages of reaction (Fig. 1A) giving rise to each of these states are indicated. (C) Representative time trace of a productive recombination event.

BS-S Complexes Are Preferentially Assembled. In the above experiment, we also observed events that showed PSF width changes without a concurrent FRET signal (42 of 6,548). These events can be attributed to DNA molecules recombined faster than our temporal resolution (200 ms) or to synaptic complexes that do not show a significant FRET in the BS FRET substrate (e.g., TS-S complexes; Fig. S4).

To obtain the fraction of recombination events missed due to our temporal resolution, we extrapolated the dwell-time distribution of productive FRET events (Fig. 3A, Right Inset; SI Text) and estimated the fraction missed to be $\sim 16\%$ of all recombination events. As this value did not account for all events that did not exhibit FRET, we constructed a second DNA substrate (TS FRET; Fig. S1) that produced a FRET signal upon formation of TS-S (but none in the BS-S complex). Using this substrate, we observed infrequent formation of TS-S ($P \approx 4.55 \times 10^{-5} \text{ s}^{-1}$; 9 of 1,212 molecules), with $\sim 50\%$ proceeding through recombination. Moreover, most recombination events did not show FRET, indicating recombination through BS-S. These results demonstrate that BS

synaptic complexes are formed preferentially over TS complexes by a factor of $\sim 8:1$.

Nonproductive Complexes. Analysis of nonproductive complexes (i.e., transient FRET, followed by return to a broad PSF; 48 molecules) revealed two distinct populations (Fig. 3B, Right). Approximately 30% of complexes show $E^* = 0.43 \pm 0.015$ (mean of fitted Gaussian and SEM); after corrections (20), this FRET efficiency corresponds to an interfluorophore distance of $64 \pm 5 \text{ \AA}$ (SI Text; Table S1). This distance agrees well with the distances in crystal structures of BS-S and BS-HJ (21), which predict a distance of $\sim 61 \text{ \AA}$ (Fig. 1C; SI Text). The remaining nonproductive complexes ($\sim 70\%$) correspond to a population with E^* of 0.26 ± 0.023 and interfluorophore distance of $75 \pm 7 \text{ \AA}$ (Table S1). This distance is significantly longer than that predicted from crystal structures (21), suggesting that, in solution, Cre can form complexes with a different architecture from the structure adopted in crystals.

To link the observed intermediates with stages of the reaction, we tested three Cre mutants: A36V, shown to be partially defective in synapsis but competent in HJ resolution (21, 22); A312T,

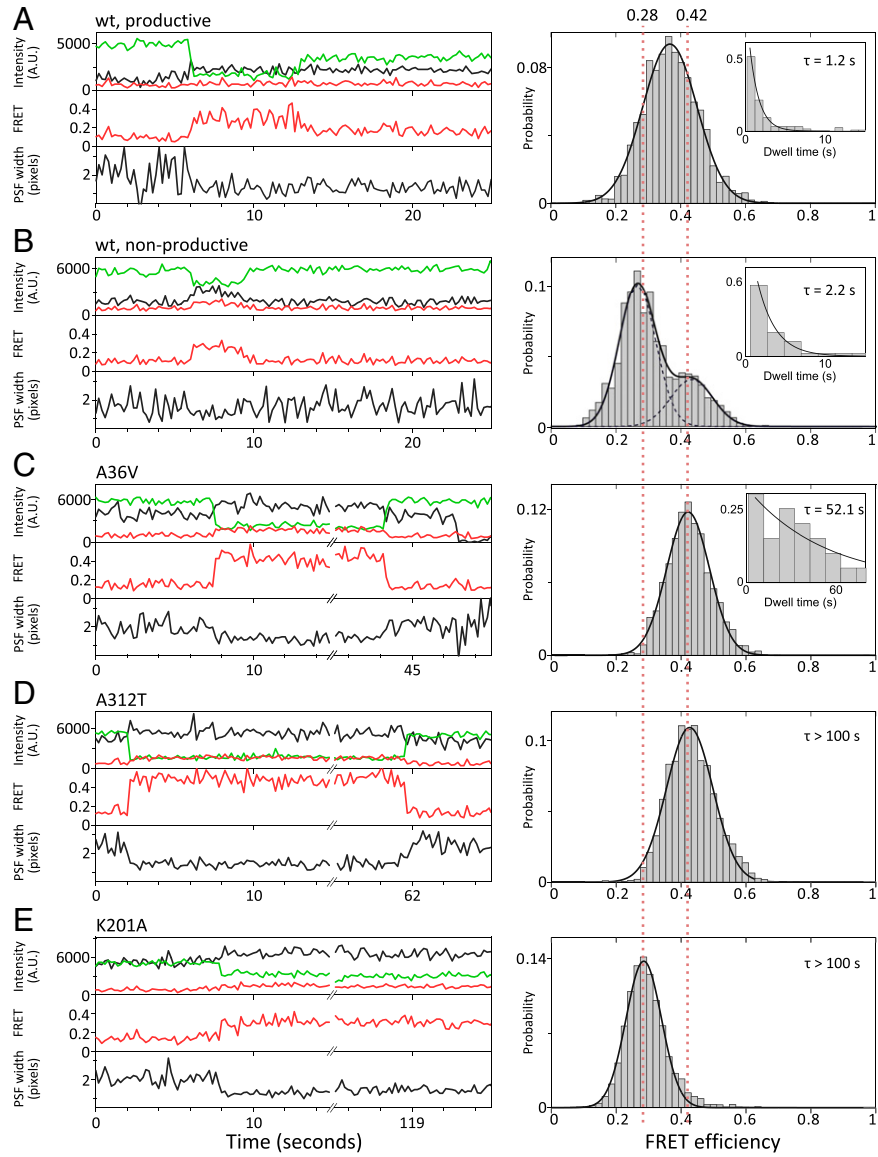


Fig. 3. FRET efficiency histograms of protein–DNA complexes for wild-type Cre and mutants. Example time traces and population histograms for (A) wt Cre productive events (91 molecules), (B) wt Cre nonproductive synaptic complex events (48 molecules), (C) Cre A36V (27 molecules), (D) Cre A312T (25 molecules), and (E) Cre K201A (86 molecules). Histograms were plotted with E^* values from each frame of an event, counts added to the histogram were normalized by the length of the event to more accurately represent the population of molecules, and histogram area was normalized to one (SI Text). Guidelines of $E^* = 0.42$ and 0.28 , corresponding to the expected BS-HJ FRET efficiency and that measured for the K201A mutant, respectively, are shown as red dotted lines. Dwell times of molecules in A, B, and C were fit to single exponentials (insets, mean lifetimes shown). D and E show very stable complexes, and dwell times could not be measured over the duration of our experiments.

known to be proficient in synapsis and first strand exchange but inefficient in recombination, thus accumulating HJs during reactions (7); and K201A, defective in DNA cleavage but proficient in synaptic complex formation (6). We confirmed the defects of these mutants in recombination (Fig. S3) and used TFM-FRET to assess their ability to proceed through the reaction. We observed frequent synaptic complex formation with A36V ($P \approx 4.5 \times 10^{-4} \text{ s}^{-1}$; $\tau \approx 52.1 \text{ s}$), with $E^* = 0.42 \pm 0.018$ (Fig. 3C), a value that corresponds well to the higher FRET species seen in the nonproductive complexes of wt Cre and in crystal structures (21). Despite forming synapses, the A36V mutant never completed recombination in our assays. Because A36V can resolve HJs (22), we propose that the main state formed by this mutant is likely to be the BS-S, rather than the BS-HJ, complex.

The A312T mutant formed stable complexes ($\tau > 100 \text{ s}$; Fig. 3D, Left) with a frequency ($P \approx 5.1 \times 10^{-4} \text{ s}^{-1}$) similar to A36V and $E^* = 0.42 \pm 0.021$ (Fig. 3D, Right). Because the E^* value for A312T matches that of A36V and the existing BS-HJ crystal structure, we conclude that A312T forms mainly BS-HJs.

Finally, the K201A mutant formed stable synaptic complexes ($P \approx 7.83 \times 10^{-4} \text{ s}^{-1}$; $\tau > 100 \text{ s}$; Fig. 3E, Left), with $E^* = 0.28 \pm 0.009$ (Fig. 3E, Right), corresponding to an interfluorophore

distance of $74 \pm 7 \text{ \AA}$. This value is surprising, as crystallographic studies have shown that the K201A mutant interacts with *loxP* sites to form a synaptic complex that is almost identical to the canonical BS conformation (21). It has previously been suggested that Lys201 plays a role in organizing the unsynapsed Cre-*loxP* complex into a cleavage-proficient conformation, which the K201A mutant may be unable to achieve (6, 8). Because it has been shown that crystallization conditions can alter the behavior of Cre mutants Y324F and R173K (21), we suggest that the discrepancy between our results and crystal structures could be due to crystal packing effects suppressing a structural defect of K201A. Intriguingly, the E^* of K201A complexes matches that of the low-FRET nonproductive complexes observed with wt Cre (Fig. 3B, Right); although we cannot conclude the equivalence or structure of the two on the basis of a single FRET value, we suggest that both may represent the same nonrecombinogenic conformation, which could represent an out-of-plane twist of the HJ arms.

Evidence for Fast Interconversions Between HJ Isomers. Analyzing productive complexes (Fig. 3A) that exhibit more than two frames of transient FRET (91 molecules), we observed a FRET distribution with mean $E^* = 0.36 \pm 0.013$ (Fig. 3A, Right), significantly

(P value < 0.01) lower than that observed for A312T and A36V ($E^* = 0.42$; Fig. 3 C and D, Right).

In addition, the width of the FRET distribution for productive complexes ($SD = 0.085 \pm 0.006$; Fig. 3A, Right) is significantly greater than the width observed for A312T and A36V ($SD \approx 0.07$; Fig. 3 C and D, Right; Table S2). Because FRET distributions from ensembles of single molecules are broadened due to intermolecular heterogeneity (23), we cannot rely on simple comparisons of the observed width with that expected on the basis of the statistical nature of photon emission ("shot-noise"). However, because photon counts throughout our studies are similar, it is likely that the excess FRET width in the case of productive complexes is a result of structural dynamics that cause unresolved FRET fluctuations. Specifically, because the reaction requires HJ isomerization before second strand exchange (Fig. 1A), we suggest that this broadening, along with the shift to a lower mean E^* than that expected for the BS-HJ, reflects isomerization of the BS-HJ ($E^* \approx 0.42$) to TS-HJ ($E^* \approx 0.18$) occurring reversibly at timescales faster than our exposure time (100 ms).

To further explore the proposed interconversion between HJ isomers, we performed Monte Carlo simulations to infer information about the underlying process (24). Assuming a population of molecules undergoing transitions between BS-HJ and TS-HJ (SI Text), we estimate an equilibrium bias of 3:1 toward the BS-HJ and forward and backward rates in the range of $20\text{--}40\text{ s}^{-1}$ and $50\text{--}100\text{ s}^{-1}$, respectively, as these parameters best recapitulate the observed distributions (SI Text; Figs. S5 and S6). This bias may reflect the asymmetric DNA sequence of the *loxP* site central region, as this region affects the conformation of HJs assembled by the related recombinase XerCD (25).

Recombinant Product Synaptic Complex Is Extremely Stable. Using the BS-FRET substrate (Fig. 2A and Fig. S1), we could not distinguish between the recombinant product complex (TS-P) and free recombinant DNA, as they have the same TFM-FRET signature (Fig. 2A, pink panels). To probe the stability of TS-P, we used a substrate with inverted *loxP* sites (Fig. S1); although recombination within this substrate inverts the DNA segment between *loxP* sites without producing a FRET signal, complex assembly and dissociation can be followed through changes in PSF width (Fig. S7A). Using this substrate, we observed that complexes were stable for longer than the 2-min acquisition time of our experiments (Fig. S7 B and C), suggesting the TS-P complex is very stable.

To further characterize the stability of TS-P (Fig. 1A), we followed its dissociation using a fluorescence correlation spectroscopy (FCS) assay (Fig. 4; SI Text). Using FCS, we monitored changes in translational diffusion as our BS FRET substrate was converted, via recombination, from a long DNA substrate (1,087 bp; diffusion coefficient, $D \approx 0.24 \times 10^{-6}\text{ cm}^2\cdot\text{s}^{-1}$) to a short DNA product (61 bp; $D \approx 0.92 \times 10^{-6}\text{ cm}^2\cdot\text{s}^{-1}$; SI Text), reflecting dissociation of the TS-P complex to free product DNA. To monitor TS-P dissociation after recombination, we measured the change in diffusion coefficient over time; in parallel, we measured diffusion in aliquots quenched with SDS (to disrupt protein interactions), evaluating progress of the reaction irrespective of TS-P dissociation (Fig. 4A).

Whereas SDS-quenched reactions displayed a rapid decrease in the fraction of substrate (similar to previous observations; ref. 18), the native reaction showed a much slower decrease, indicating that TS-P dissociation occurs at a much slower timescale (Fig. 4B). Single-exponential fits give rates of 0.01 min^{-1} and 0.96 min^{-1} for native and SDS-quenched reactions, respectively, indicating that the lifetime of the TS-P complex is ~ 75 min. Our dissociation rates agree with those derived from a kinetic model of Cre recombination (18) and previous observations of highly stable complexes (26, 27).

Discussion

Here we report single-molecule fluorescence views of Cre recombination. Using our assay, TFM, in conjunction with FRET, we observe single recombination reactions in real time using wt

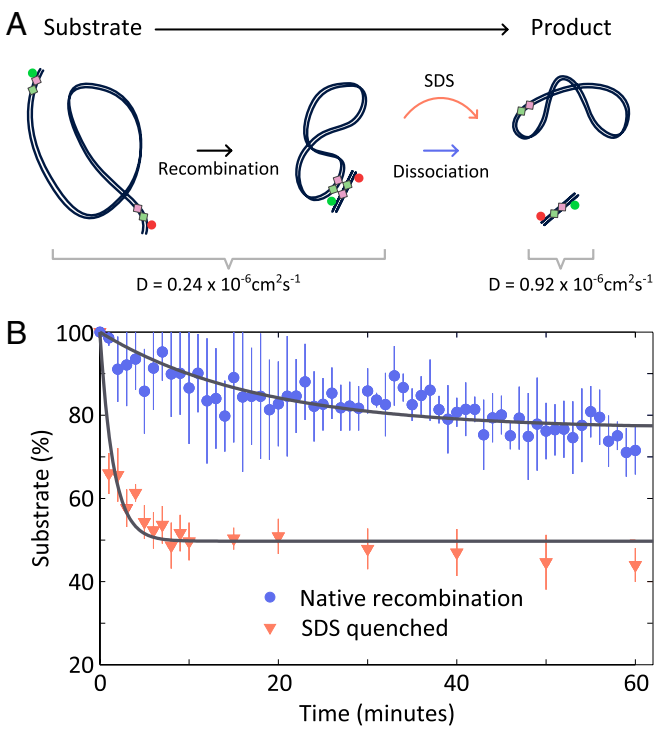


Fig. 4. Stability of product synaptic complex. (A) Schematic of the FCS assay used to investigate kinetics of TS-P dissociation. Dissociation, which can either occur naturally or be induced by addition of SDS, leads to an increase in the diffusion coefficient of the labeled species. (B) Progress of native (blue) or SDS quenched (red) recombination reactions over time.

Cre and native *loxP* sites. The single-molecule nature of TFM-FRET provides direct access to transient reaction intermediates and reaction paths, while uncovering molecular heterogeneity.

TFM Assay for Observing Real-Time Cre Recombination. TFM allows observation of large-scale conformational changes of DNA, analogous to TPM (28), but without the perturbing effect of a large bead (29). The dual role of the surface-distal fluorophore (as a reporter of surface proximity and as a FRET acceptor) enables simultaneous FRET measurements that detect subtle conformational changes at the nanometer scale; as a result, the temporal coupling of global and local changes can be examined. Importantly, the FRET efficiency helps the assignment of observed intermediates to conformations seen in crystal structures. TFM is applicable to most processes involving large DNA deformations, such as looping, condensation, and changes in persistence length. On a practical note, TFM can be implemented on any single-molecule TIRF microscope without any modification.

Using TFM-FRET, we were able to identify conformational states formed during individual recombination reactions and analyze their conversion kinetics. In addition to following complete reactions, we also identified molecules that progress only partially through recombination.

Reaction Paths and a Unique Intermediate. The direct observation of intermediates allowed us to shed light on Cre-*loxP* recombination. Previous work has shown a preference for recombination via BS exchange (6–8), and we confirmed that this preference arises because of an eightfold bias toward BS synaptic complex formation, rather than major differences in recombination efficiency in BS and TS complexes (BS $\approx 75\%$, TS $\approx 50\%$). We also showed that, alongside assembly of the canonical BS structure, wild-type Cre (and K201A) can form, previously unobserved, nonproductive complexes with a structure distinct from those captured in crystals. Although the role

of such complexes is not clear, their existence needs to be considered in any ensemble kinetic studies of Cre recombination.

Rate-Limiting Step for Productive Complexes. Our results establish that, once formed, synaptic complexes proceed rapidly through the reaction. For productive complexes, we measured the lifetime of the transient FRET state of $E^* \approx 0.36$ (representing a mixture of BS-S, BS-HJ, and TS-HJ) to be ~ 1.2 s. The single-exponential decay of the dwell times in this state points to a single rate-limiting step before further progress through the reaction. Because this FRET state reflects, in part, the interconversion between HJ complexes, we conclude that the rate-limiting step is concurrent with or occurs after HJ isomerization. This rate-limiting step could be the second DNA strand exchange or a conformational change that ends HJ isomerization and/or changes the activity of the Cre monomers. We compare this to a study on λ Int (which, in contrast to Cre, requires accessory proteins) that observed that a rate-limiting step occurred before, or concomitant with, HJ formation (4).

HJ Dynamics. In productive complexes we observed the presence of previously undetected dynamics of the HJ intermediates, estimating isomerization rates of $10\text{--}100\text{ s}^{-1}$. Intriguingly, these values are similar to rates observed for transitions between protein-free HJ conformers ($20\text{--}100\text{ s}^{-1}$; ref. 30), suggesting that, although Cre affects the structure of the HJs formed (31), it does not substantially affect the isomerization rate. In contrast, we see no appreciable interconversion between HJ isomers using the A312T mutant, indicating that this mutant favors the BS conformation, either due to a change in isomerization rates between HJ isomers or due to an alteration in HJ cleavage proficiencies. Although from published biochemical data we do not expect that the A36V mutant will appreciably populate the HJ state, we cannot rule out that if it is able to form a HJ, it may also be undergoing some biased HJ isomerization (with the equilibrium being heavily shifted toward the BS-HJ form).

Stable Recombinant Synaptic Complexes. After completion of recombination, we observed long-lived recombinant product synaptic complexes (TS-P) refractory to subsequent recombination. This

lifetime agrees with ensemble measurements (26, 27) but is significantly longer than observed in a TPM study (12); however, we note that the use of a 200-nm bead in the TPM work generates an effective stretching force on the DNA (29) and may have increased the rate of complex dissociation. Previous ensemble biochemical data had measured similar dissociation constants (K_d) for the synaptic complexes of wt Cre and K201A (14 and 9 nM, respectively; ref 21). In our case, we observe that wt Cre complexes quickly form the TS-P complex ($\tau \approx 1.2$ s, Fig. 3A), whereas those formed by K201A are very stable ($\tau > 100$ s). Unlike the ensemble assay, we were able to distinguish between BS-S and TS-P wt complexes, observing that BS-S is transient and TS-P is highly stable. Our results indicate that the previous K_d measurements for wt Cre were dominated by the TS-P complex rather than the BS-S complex (21). Our results also show that the K_d of >500 nM for the A36V synaptic complex (21) does not indicate a deficiency in complex formation but instead a ~ 100 -fold reduction in the complex stability, compared with wt Cre TS-P. The broadly similar association probabilities (and thus on-rates) we estimated indicate that, under our conditions, synapse formation is likely to be a diffusion-limited process. We note that, although TS-S and TS-P (i.e., TS complexes formed as either the substrate or product of the recombination reaction) could naively be assumed to be identical, our results indicate significant differences in the stability of each. This difference between complexes suggests an intriguing avenue for further study, which may shed further light on the mechanisms of regulation within Cre-*loxP* recombination.

Materials and Methods

Standard techniques for DNA labelling and protein purification were used and are described in detail in *SI Text*. Single-molecule and FCS experiments are described in *SI Text*. Details and procedures for data analysis and accurate FRET and distance calculation and simulations are also presented in *SI Text*.

ACKNOWLEDGMENTS. We thank Gregory Van Duyne for plasmids for Cre overexpression. J.N.M.P. was supported by the UK Engineering and Physical Sciences Research Council. A.N.K. was supported by European Commission Seventh Framework Programme Grant FP7/2007-2013 HEALTH-F4-2008-201418, Biotechnology and Biological Research Council Grant BB/H01795X/1, and European Research Council Starter Grant 261227. Work in the D.J.S. laboratory was supported by Wellcome Trust Program Grant WT083469MA.

- Grindley NDF, Whiteson KL, Rice PA (2006) Mechanisms of site-specific recombination. *Annu Rev Biochem* 75:567–605.
- Van Duyne GD (2001) A structural view of cre-*loxP* site-specific recombination. *Annu Rev Biophys Biomol Struct* 30:87–104.
- Grainge I, Lesterlin C, Sherratt DJ (2011) Activation of XerCD-dif recombination by the FtsK DNA translocase. *Nucleic Acids Res* 39(12):5140–5148.
- Mumm JP, Landy A, Gelles J (2006) Viewing single lambda site-specific recombination events from start to finish. *EMBO J* 25(19):4586–4595.
- Sauer B (1993) Manipulation of transgenes by site-specific recombination: use of Cre recombinase. *Guide to Techniques in Mouse Development*, eds Wassarman PM, DePamphilis ML (Academic Press, Waltham, MA), Vol 225, pp 890–900.
- Ghosh K, Lau C-K, Gupta K, Van Duyne GD (2005) Preferential synapsis of loxP sites drives ordered strand exchange in Cre-*loxP* site-specific recombination. *Nat Chem Biol* 1(5):275–282.
- Hoess R, Wierzbicki A, Abremski K (1987) Isolation and characterization of intermediates in site-specific recombination. *Proc Natl Acad Sci USA* 84(19):6840–6844.
- Lee L, Sadowski PD (2003) Sequence of the loxP site determines the order of strand exchange by the Cre recombinase. *J Mol Biol* 326(2):397–412.
- Ennifar E, Meyer JEW, Buchholz F, Stewart AF, Suck D (2003) Crystal structure of a wild-type Cre recombinase-*loxP* synapse reveals a novel spacer conformation suggesting an alternative mechanism for DNA cleavage activation. *Nucleic Acids Res* 31(18):5449–5460.
- Martin SS, Pulido E, Chu VC, Lechner TS, Baldwin EP (2002) The order of strand exchanges in Cre-*LoxP* recombination and its basis suggested by the crystal structure of a Cre-*LoxP* Holliday junction complex. *J Mol Biol* 319(1):107–127.
- Vetcher AA, et al. (2006) DNA topology and geometry in Flp and Cre recombination. *J Mol Biol* 357(4):1089–1104.
- Fan H-F (2012) Real-time single-molecule tethered particle motion experiments reveal the kinetics and mechanisms of Cre-mediated site-specific recombination. *Nucleic Acids Res* 40(13):6208–6222.
- Bai H, et al. (2011) Single-molecule analysis reveals the molecular bearing mechanism of DNA strand exchange by a serine recombinase. *Proc Natl Acad Sci USA* 108(18):7419–7424.
- Kapanidis AN, et al. (2004) Fluorescence-aided molecule sorting: Analysis of structure and interactions by alternating-laser excitation of single molecules. *Proc Natl Acad Sci USA* 101(24):8936–8941.
- Kapanidis AN (2008) Alternating-laser excitation of single molecules. *Single Molecule Techniques: A Laboratory Manual*, eds Selvin PR, Ha T (Cold Spring Harbor Laboratory Press, Cold Spring Harbor, NY), 1st Ed, pp 85–119.
- Nelson PC, et al. (2006) Tethered particle motion as a diagnostic of DNA tether length. *J Phys Chem B* 110(34):17260–17267.
- Axelrod D (1981) Cell-substrate contacts illuminated by total internal reflection fluorescence. *J Cell Biol* 89(1):141–145.
- Ringrose L, et al. (1998) Comparative kinetic analysis of FLP and cre recombinases: Mathematical models for DNA binding and recombination. *J Mol Biol* 284(2):363–384.
- Lee L, Sadowski PD (2001) Directional resolution of synthetic Holliday structures by the Cre recombinase. *J Biol Chem* 276(33):31092–31098.
- Lee NK, et al. (2005) Accurate FRET measurements within single diffusing biomolecules using alternating-laser excitation. *Biophys J* 88(4):2939–2953.
- Ghosh K, Guo F, Van Duyne GD (2007) Synapsis of loxP sites by Cre recombinase. *J Biol Chem* 282(33):24004–24016.
- Lee L, Sadowski PD (2003) Identification of Cre residues involved in synapsis, isomerization, and catalysis. *J Biol Chem* 278(38):36905–36915.
- Holden SJ, et al. (2010) Defining the limits of single-molecule FRET resolution in TIRF microscopy. *Biophys J* 99(9):3102–3111.
- Santoso Y, et al. (2010) Conformational transitions in DNA polymerase I revealed by single-molecule FRET. *Proc Natl Acad Sci USA* 107(2):715–720.
- Arciszewska LK, Baker RA, Hallett B, Sherratt DJ (2000) Coordinated control of XerC and XerD catalytic activities during Holliday junction resolution. *J Mol Biol* 299(2):391–403.
- Hamilton DL, Abremski K (1984) Site-specific recombination by the bacteriophage P1 *lox*-Cre system. Cre-mediated synapsis of two lox sites. *J Mol Biol* 178(2):481–486.
- Shoura MJ, et al. (2012) Measurements of DNA-loop formation via Cre-mediated recombination. *Nucleic Acids Res* 40(15):7452–7464.
- Schafer DA, Gelles J, Sheetz MP, Landick R (1991) Transcription by single molecules of RNA polymerase observed by light microscopy. *Nature* 352(6334):444–448.
- Segall DE, Nelson PC, Phillips R (2006) Volume-exclusion effects in tethered-particle experiments: Bead size matters. *Phys Rev Lett* 96(8):088306–088310.
- McKinney SA, Déclais A-C, Lilley DMJ, Ha T (2003) Structural dynamics of individual Holliday junctions. *Nat Struct Biol* 10(2):93–97.
- Gopaul DN, Guo F, Van Duyne GD (1998) Structure of the Holliday junction intermediate in Cre-*loxP* site-specific recombination. *EMBO J* 17(14):4175–4187.

Supporting Information

Pinkney et al. 10.1073/pnas.1211922109

SI Text

DNA and Protein Preparation. Mutants of Cre were prepared with QuikChange Site-Directed Mutagenesis Kit (Stratagene), and tagless proteins were purified, according to Ghosh et al. (1), and their identities were confirmed with mass spectroscopy. A total of 1,087 bp DNA substrates were prepared via a PCR using two fluorescently labeled oligonucleotides as primers and a plasmid template containing directly repeated *loxP* sites separated by a 1 kb Km^R gene (pRB10*loxP*) and Phusion High-Fidelity DNA polymerase (NEB). Two oligonucleotides were used: forward 5'-tgcatacgatcatcaX-aacttcgtat-3' and reverse 5'-gtggatccacXtgataacttcgtat-3', where X indicates the position of 5-C6-amino dT; additionally, the 5' end of the reverse oligonucleotide was labeled with biotin. Forward and reversed oligonucleotides were labeled at X positions with Cy5 and Cy3B, respectively. Oligonucleotides were synthesized and HPLC purified by ATDBio Ltd. Cy5 labeling was performed by ATDBio, whereas Cy3B labeling was performed as previously described (2). After PCR reactions, the product was gel-purified.

Instrumentation. Single-molecule TIRF experiments were performed on a custom-built objective type TIRF microscope. A green (532 nm Cobolt Samba) and red (635 nm Cube Coherent) laser were combined using a dichroic mirror and coupled into a fiber optic cable. The output of the fiber was focused into the back focal plane of the objective (100× oil immersion, numerical aperture 1.4, Olympus) and displaced perpendicular to the optical axis such that laser light was incident at the slide-solution interface at greater than the critical angle, creating an evanescent excitation field. ALEX (2) was implemented by directly modulating the lasers, and all data were acquired using a 100 Hz alternation rate, with excitation powers of 1 mW for each laser. Fluorescence emission was collected by the objective and separated from the excitation light by a dichroic (545 nm / 650 nm, Semrock) and cleanup filters (545 nm LP, Chroma; and 633/25 nm notch filter, Semrock). Emission signal was focused on a rectangular slit to crop the image and then spectrally separated, using a dichroic (630 nm DRLP; Omega), into two emission channels which were focused side by side onto an EMCCD camera (Andor iXon 897). The EMCCD was set to an EM gain of 300, corresponding to an approximate real gain of 4.55 counts per photon.

Sample Preparation. Biotinylated DNA was immobilized to the surface of a PEG-passivated coverslip using biotin–neutravidin interactions and sealed using a silicone gasket (Grace Bio-laboratories) and a second coverslip as a lid. Imaging was performed in a buffer consisting of 50 mM Tris-HCl (pH 7.5), 50 mM NaCl, 5 mM MgCl₂, 100 µg·mL⁻¹ BSA, and 1 mM UV-treated Trolox. An enzymatic oxygen scavenging system consisting of 1 mg·mL⁻¹ glucose oxidase, 40 µg·mL⁻¹ catalase, and 1.4% (wt/vol) glucose was added just before sealing the sample before image acquisition. All experiments were performed at a room temperature of 21 °C. In experiments where SDS was used to disrupt protein interactions, it was added to the buffer at a concentration of 0.1%.

Data Analysis. Extraction of fluorescence intensity signals from microscope images was performed by the previously described TwoTone software (3). An apparent FRET efficiency, E^* , was calculated from the extracted fluorescence emission:

$$E^* = \frac{F_{DA}}{F_{DD} + F_{DA}},$$

and the acceptor PSF width was obtained from the mean width of the fitted elliptical Gaussian.

Further analysis and quantification of extracted signals was performed with custom-written MATLAB software. For analysis of recombination events, intensity traces from individual molecules was manually inspected and classified. Transient FRET signals were defined on the basis of $E^* > 0.2$ along with the appropriate changes in PSF width and acceptor intensity; in the case of events that returned to substrate, short events (less than two frames) were discarded as these could not reliably be distinguished from fluctuations due to noise. However, in the case of “productive” events, unambiguous PSF and intensity signals allowed assignment of events that displayed short or no transient FRET. Any molecules whose fluorophores bleached within 10 s of a FRET event or that exhibited confounding photophysical fluctuations were excluded from the analysis. Under our imaging conditions, we measure the lifetimes of Cy3B and Cy5 to be ~400 s and 160 s, respectively (fit to single exponential decay), and that ~10% of molecules show errant photophysics from either fluorophore. Further, ~5% of molecules were observed with two-step photobleaching or intensities corresponding to more than one fluorophore at a single localization position, and these were discarded.

Histograms of E^* values were constructed by extracting the manually assigned FRET frames, discarding the first and last frames, and plotting the data points to a histogram, normalizing each count by the length of the observed event.

FCS Experiments. FCS was carried out on a ConfoCor 3 system (Carl Zeiss). The 633 nm line of a HeNe laser was directed via 488/561/633 dichroic mirror and focused with a Zeiss C-Apo-chromat 40× NA 1.2 water immersion objective to excite experimental samples containing Cy5. Fluorescence emission was collected using a 655-nm longpass filter and recorded by a set of avalanche photodiodes. The pinhole diameter was adjusted to 83 µm (one Airy unit), and the pinhole position was optimized with use of the automatic pinhole adjustment for Cy5.

FCS measurements were conducted for BS FRET substrate (Fig. S24) in the presence of 0.05% SDS as well as without the detergent. The SDS concentration used was below the cpc (critical micelle concentration = 8.15×10^{-3} M, whereas the 0.05% SDS used in our studies corresponds to 1.7×10^{-3} M), and we did not observe any change in diffusion upon SDS addition.

To acquire kinetics of the recombination reaction and dissociation of product DNAs, we performed reactions in solution where 2 nM of the BS FRET substrate were mixed with 320 nM Cre protein. To avoid rebinding of short product DNA back to the BS FRET substrate, an excess of a *loxP* containing short oligonucleotide (100 nM) was present as a competitor. It should be noted that in the case of intermolecular reactions between the BS FRET substrate and short oligonucleotide, the resulting product will have very similar length to that produced by intramolecular reactions (58 bp and 60 bp, respectively), which will have no appreciable effect on the change in diffusion time. During the course of the experiment, decrease in diffusion time was analyzed as a function of product dissociation after completion of recombination. It is worth noting that only molecules that completed all chemistry steps and then dissociated would result in a decreased diffusion time, whereas nonproductive synaptic complexes and reactions stuck at the HJ stage would have no effect. To analyze the stability of a complex after all chemistry was completed, we prepared a volume of 500 µL

of the reaction mixture containing Cre, BS FRET substrate, and oligonucleotide. Then a 50 μL volume was put in a glass chamber to perform 60 \times 1-min FCS measurements. The rest of the mixture was used to analyze the change in diffusion coefficient using SDS to disrupt any protein–protein and protein–DNA interactions. Any difference in diffusion time between samples quenched with SDS and those in native conditions would be the result of stability of product DNA before dissociation. For this purpose 19 μL was taken from the reaction mixture and stopped by addition of 1 μL 1% SDS. The Cre-*loxP* reaction was stopped minute-by-minute for the first 10 min, then at 15, 20, 30, 40, 50, and 60 min of incubation in 22 °C. The reference sample used to calculate diffusion coefficient was BS FRET substrate with SDS.

Samples quenched with SDS were measured 5 \times 10 s. All FCS experiments were carried out in Lab-Tek (Nagle Nunc International) eight-well chambered borosilicate glass plates at 22 ± 1 °C.

FCS Data Analysis. In FCS experiments the intensity of fluorescence signal is measured and the autocorrelation function $G(t)$ is determined for diffusing fluorophores present in the sample. Here, $G(t)$ can be expressed as a two-component model (4):

$$G(\tau) = \left[1 - T + T \exp\left(\frac{-\tau}{\tau_T}\right) \right] N^{-1} \times \left[\frac{1 - Y}{\left(1 + \frac{\tau}{\tau_{substrate}}\right) \sqrt{1 + \frac{r_0^2}{z_0^2} \frac{\tau}{\tau_{substrate}}}} + \frac{Y}{\left(1 + \frac{\tau}{\tau_{product}}\right) \sqrt{1 + \frac{r_0^2}{z_0^2} \frac{\tau}{\tau_{product}}}} \right],$$

where T is the average fraction of dye molecules in the triplet state with the relaxation time τ_T , N is the average number of fluorescent molecules in the volume observed, Y is the relative fraction of released product DNA, $\tau_{substrate}$ and $\tau_{product}$ are the diffusion time constants of substrate DNA and product DNA, respectively, and r_0 and z_0 are the lateral and axial dimension respectively of the observation volume. The diffusion coefficient can be determined by calibrating the experiment using a standard dye, in our case Cy5 ($D = 3.7 \times 10^{-6} \text{ cm}^2 \cdot \text{s}^{-1}$; ref. 5). Diffusion coefficients for any labeled DNA can then be calculated according to the relation:

$$D_x = \frac{\tau_{Cy5}}{\tau_x} D_{Cy5},$$

where D_{Cy5} is the diffusion coefficient, τ_{Cy5} is the correlation time of Cy5 (55 μs), and D_x and τ_x are the diffusion coefficient and correlation time for the labeled DNA. We calculated diffusion coefficients of the BS FRET substrate and product DNA to be $0.24 \times 10^{-6} \text{ cm}^2 \cdot \text{s}^{-1}$ and $0.92 \times 10^{-6} \text{ cm}^2 \cdot \text{s}^{-1}$, respectively.

The correlation time of the BS FRET substrate was determined assuming a one-component model. The correlation time of the product DNA was obtained by fitting an overnight recombination reaction stopped with SDS to a two-component model with fixed time for BS FRET substrate and the second component left free. During the analysis of experiments, the correlation times for BS FRET substrate and product DNA were fixed at measured values. All of the calculations, including the evaluation of the autocorrelation curves, which was carried out with a Marquardt nonlinear least-square fitting procedure, were performed using the software of the ConfoCor 3 instrument.

Quantifying Complex Formation Frequency. To quantify the frequency of complex formation events we calculate a probability of complex formation per particle, by dividing the total number of

events observed by the initial number of substrate molecules in a given movie. To account for the varying length of our movies, for example due to cessation caused by focal drift, we divide this probability by the mean movie length to obtain an approximate probability of complex formation per particle per unit time. This calculation assumes that all substrate molecules are available to participate in reactions and that photo-bleaching is not a major factor over the timescales for which we observe. These assumptions likely do not hold for our surface-immobilized DNAs and 100-s movies, so we cannot use this probability to accurately infer information about the absolute on-rate of complex formation. However, the above effects are equivalent over all our experimental conditions, so we can reliably compare this value between experiments to determine the relative frequency of complexes formed. We also note that very short-lived synaptic complexes are likely to be missed due to our temporal resolution of 100 ms; thus, the probability values given in the case of synaptic complex formation are likely to be lower limits.

Accurate FRET and Distance Calculation. We follow previously described procedures for obtaining accurate FRET (6). Briefly, we correct for donor leakage into the acceptor emission channel, l ; direct excitation of the acceptor by the 532 nm laser, d ; and the effect of differing quantum yields Q , and detection efficiency η , of the fluorophores, generally termed γ , to give an expression for accurate FRET given by:

$$E = \frac{DA_{correct}}{\gamma F_{DD}(1+l) + DA_{correct}},$$

where:

$$DA_{correct} = F_{DA} - lF_{DD} - dF_{AA},$$

and:

$$\gamma = \frac{Q_A \eta_A}{Q_D \eta_D}.$$

We obtain values for l and d by looking at fluorescence signals from the appropriate singly labeled short oligonucleotides. The ratio γ is determined by measuring many acceptor bleaching during FRET events observed with Cre A312T (7); the mean of these single measurements for γ is then used as a correction for all molecules.

Emission spectra of Cy3B and absorption spectra of Cy5 were measured on a fluorometer (Photon Technology International) under conditions as closely resembling those of the single-molecule experiment as possible. R_0 was calculated using the expression:

$$R_0 = 0.211(\kappa^2 n^{-4} Q_D J)^{1/6},$$

$$J = \int f_D(\lambda) \epsilon_A(\lambda) \lambda^4 d\lambda,$$

where n is the refractive index of the medium (1.33), f_D is the normalized fluorescence emission of the donor, and ϵ_A is the extinction coefficient of the acceptor. We assume a literature value of 0.67 for Q_D , the quantum yield of Cy3B (8), and that the dipole orientation factor $\kappa^2 = 2/3$. To justify our assumption of rotational freedom of the fluorophores attached to DNA, we measure their anisotropy values in the presence of wt Cre and use these to obtain an estimate for the possible range of true values for κ^2 (9). We use these errors, and the SD of our E^* and stoichiometry values, as well as estimates for the errors on the measurements of fluo-

rophore spectral properties, to perform standard propagation of errors to compute the SEM for our distance measurements, as outlined in Uphoff et al. (10) (Table S2).

To estimate the expected interfluorophore distance we extrapolate one DNA arm of the Cre-*loxP* synaptic complex structure [2HOI (11) for the BS conformation and 1 NZB (12) for the TS conformation] to encompass our labeling site. To account for the effect of linker length, we superimpose the sterically accessible region computed by Wozniak et al. (13) and use the mean fluorophore positions to estimate their separation.

Post-recombination Synaptic Complex Distance. The distance estimate from crystal structures of the TS-HJ and TS-P complex are 83 Å; measuring the FRET value after the BS complex in our “productive” complexes, we obtain a mean value of 0.18, indicating a distance of 84 ± 11 Å. Although this is measurable over the ensemble of single molecules, we refer to this as a “negligible” FRET value due to its proximity to the FRET efficiency arising solely due to spectral cross-talk in our system ($E^* = 0.13$), and consequently it is not reliably identifiable in intensity traces from individual molecules.

FRET Simulations. Simulations were performed assuming rapid interconversion between the two HJ conformers to determine if this could give rise to the observed FRET distributions. We simulated stochastic fluorophore emission from two states that were able to

interconvert faster than the frame time of acquisition using a Markov chain approach; we assigned these states to have uncorrected FRET values of 0.18 and 0.43 for the TS-HJ and BS-HJ, respectively, estimated from the 2HOI crystal structure (11). The fluorescence emission collected over a frame was then put through simulated background noise and EM gain to obtain the final emission counts in simulated data. We tune the rate of fluorophore photon emission in the simulations to produce distributions that match the observed width arising from a static FRET standard. This gives rise to photon counts that are somewhat lower than those from single molecules in our experiments to reproduce the effect of broadening due to colating an ensemble of single molecules in our FRET distributions (3).

To obtain an estimate for the rates of interconversion that could recapitulate the observed distribution, we systematically varied the forward and backward rates of HJ interconversion (Fig. S6) and performed many simulated runs for each parameter pair for a number of frames corresponding to those in the experimental data. We then fitted the output distribution using a single Gaussian and recorded the mean, variance, and the coefficient of determination of the fit. Assuming a normal distribution of parameter values for each model, we then computed the likelihood of the model given our observed data (Fig. S5). By the definition of likelihood, the parameters that maximized this value would be those that are most likely to give rise to our observed data.

1. Ghosh K, Van Duyne GD (2002) Cre-*loxP* biochemistry. *Methods* 28(3):374–383.
2. Kapanidis AN (2008) Alternating-laser excitation of single molecules. *Single Molecule Techniques: A Laboratory Manual*, eds Selvin PR, Ha T (Cold Spring Harbor Laboratory Press, Cold Spring Harbor, NY), 1st Ed, pp 85–119.
3. Holden SJ, et al. (2010) Defining the limits of single-molecule FRET resolution in TIRF microscopy. *Biophys J* 99(9):3102–3111.
4. Meyer-Almes FJ, Wyzgol K, Powell MJ (1998) Mechanism of the alpha-complementation reaction of *E. coli* beta-galactosidase deduced from fluorescence correlation spectroscopy measurements. *Biophys Chem* 75(2):151–160.
5. Loman A, Dertinger T, Koberling F, Enderlein J (2008) Comparison of optical saturation effects in conventional and dual-focus fluorescence correlation spectroscopy. *Chem Phys Lett* 459:18–21.
6. Lee NK, et al. (2005) Accurate FRET measurements within single diffusing biomolecules using alternating-laser excitation. *Biophys J* 88(4):2939–2953.
7. Ha T, et al. (1999) Single-molecule fluorescence spectroscopy of enzyme conformational dynamics and cleavage mechanism. *Proc Natl Acad Sci USA* 96(3):893–898.
8. Cooper M, et al. (2004) Cy3B: Improving the performance of cyanine dyes. *J Fluoresc* 14(2):145–150.
9. Dale RE, Eisinger J, Blumberg WE (1979) The orientational freedom of molecular probes. The orientation factor in intramolecular energy transfer. *Biophys J* 26(2):161–193.
10. Uphoff S, et al. (2010) Monitoring multiple distances within a single molecule using switchable FRET. *Nat Methods* 7(10):831–836.
11. Ghosh K, Guo F, Van Duyne GD (2007) Synapsis of *loxP* sites by Cre recombinase. *J Biol Chem* 282(33):24004–24016.
12. Ennifar E, Meyer JEW, Buchholz F, Stewart AF, Suck D (2003) Crystal structure of a wild-type Cre recombinase-*loxP* synapse reveals a novel spacer conformation suggesting an alternative mechanism for DNA cleavage activation. *Nucleic Acids Res* 31(18):5449–5460.
13. Wozniak AK, Schröder GF, Grubmüller H, Seidel CAM, Oesterhelt F (2008) Single-molecule FRET measures bends and kinks in DNA. *Proc Natl Acad Sci USA* 105(47):18337–18342.

a BS FRET substrate**b TS FRET substrate****c Inverted repeat substrate**

Fig. S1. Sequences and labeling positions of DNA substrates used throughout this study. (A) BS FRET substrate, designed to show FRET in the BS-S complex. (B) TS FRET substrate, designed to show FRET in the TS-S complex. (C) Inverted repeat substrate, used to investigate complex dissociation. *loxP* sites are indicated by dashed boxes, and the orientation by the arrows above. TSs and BSs are indicated in red and black, respectively; the long sequence of DNA linking the sites is not shown and is represented by dashed lines.

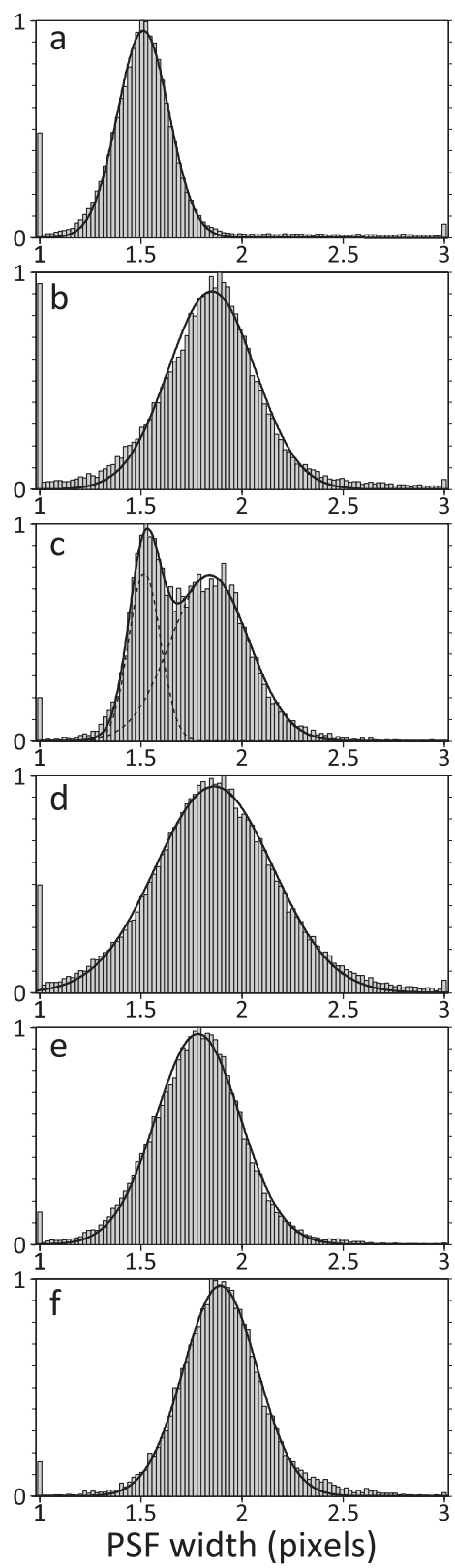


Fig. S2. End point assay to verify recombination proficiency of molecules tethered to a PEG passivated coverslip. (A) Short (80 bp) labeled DNA, (B) long (1 kb) substrate DNA molecules with no protein to act as length standards, (C–F) Long substrate DNA incubated with proteins: C, wt Cre; D, Cre K201A; E, Cre A312T; F, Cre A36V for 10 min at room temperature (22 °C). Samples were then washed with buffer, SDS, and buffer again before a final wash with imaging buffer, after which 500-frame movies from five fields of view were collected to sample the state of molecules at the surface; A shows the typical diffraction-limited PSF expected for a surface-immobilized fluorophore on the microscope; (B and D–F) exhibit broadening concomitant with the long DNA substrate; and C shows a mix of broad and narrow PSFs, indicating that ~30% of surface-immobilized molecules have undergone at least one pair of strand exchange.

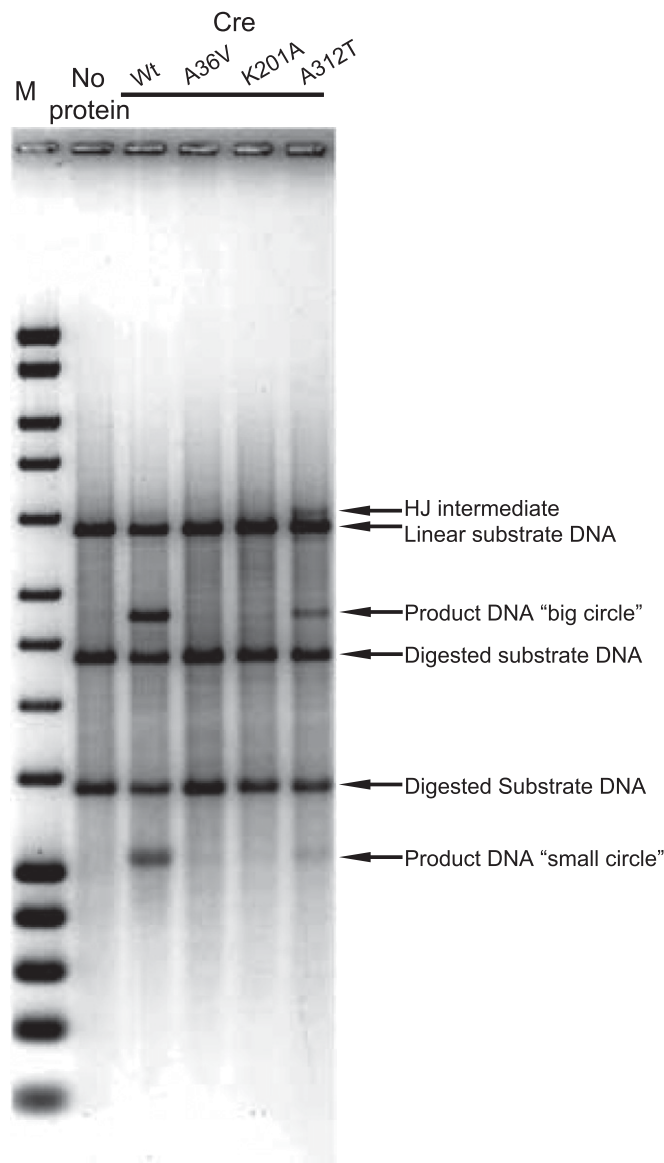
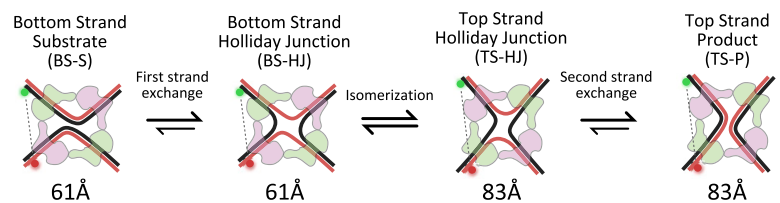


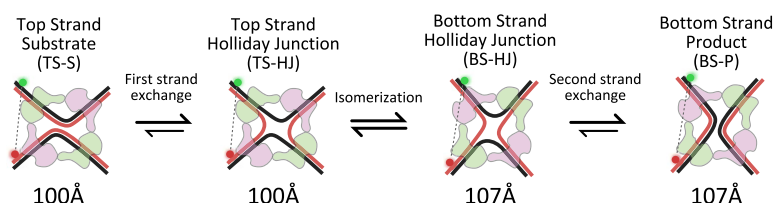
Fig. S3. Gel electrophoresis of recombination reaction carried for 10 min at 37° in buffer used thorough all studies. A 3.7 kb plasmid caring two directly repeated *loxP* sites (used as a template in PCR) was used. Product of recombination is expected to be “big” (2.7 kb) and “small” (1 kb) circles. Double digest reveal linearized products in reaction with wt and A312T mutant but none when A36V or K201A was used. As expected, A312T is less efficient in recombination and accumulates HJ intermediate.

BS-FRET substrate

a 'bottom-strand' first recombination

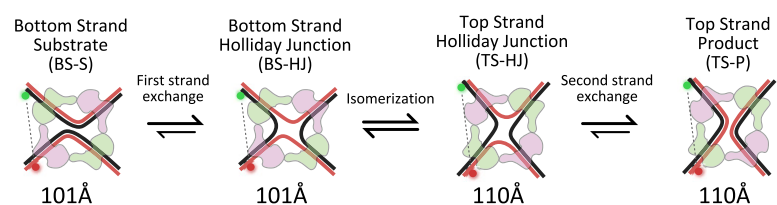


b 'top-strand' first recombination



TS-FRET substrate

c 'bottom-strand' first recombination



d 'top-strand' first recombination

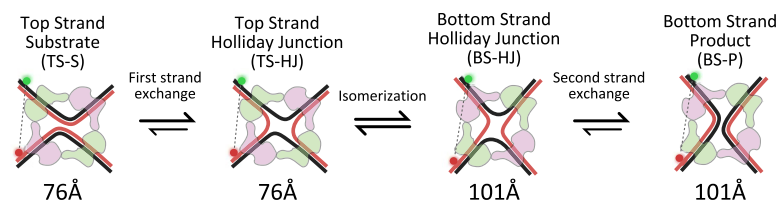


Fig. S4. Schematic comparison of the expected interfluorophore distances (as measured from crystal structures) at each stage of the reaction using either the BS-FRET substrate (A and B) or the TS-FRET substrate (C and D). For each substrate two possible reaction paths are shown: reactions can either be initiated from a substrate in which BSs are positioned to be cleaved first (A and C) or one in which TSs are cleaved first (B and D).

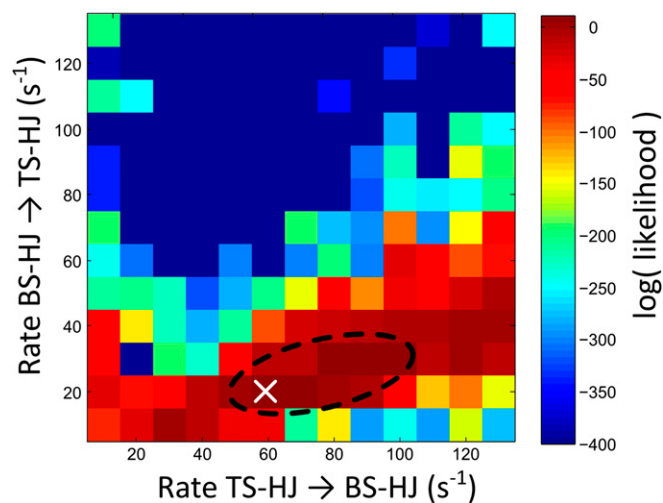


Fig. S5. Likelihood of the observed data given the distributions obtained from simulating many observations with a forward and backward rate of interconversion between HJ isomers (*SI Text*). The region of the graph giving the maximum likelihood values is outlined in black, and the pair of rates giving the maximum value is marked with a white cross.

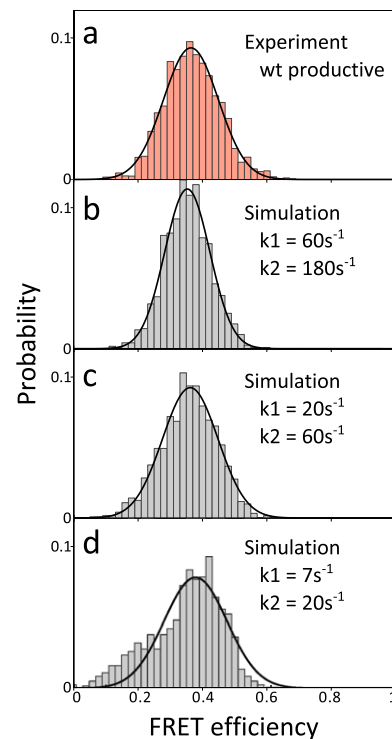


Fig. S6. Comparison of FRET efficiency distributions. (A) experimental wild-type Cre productive complex distribution and (B–D) simulated data with varying forward and backward rates of interconversion between the two HJ isomers.

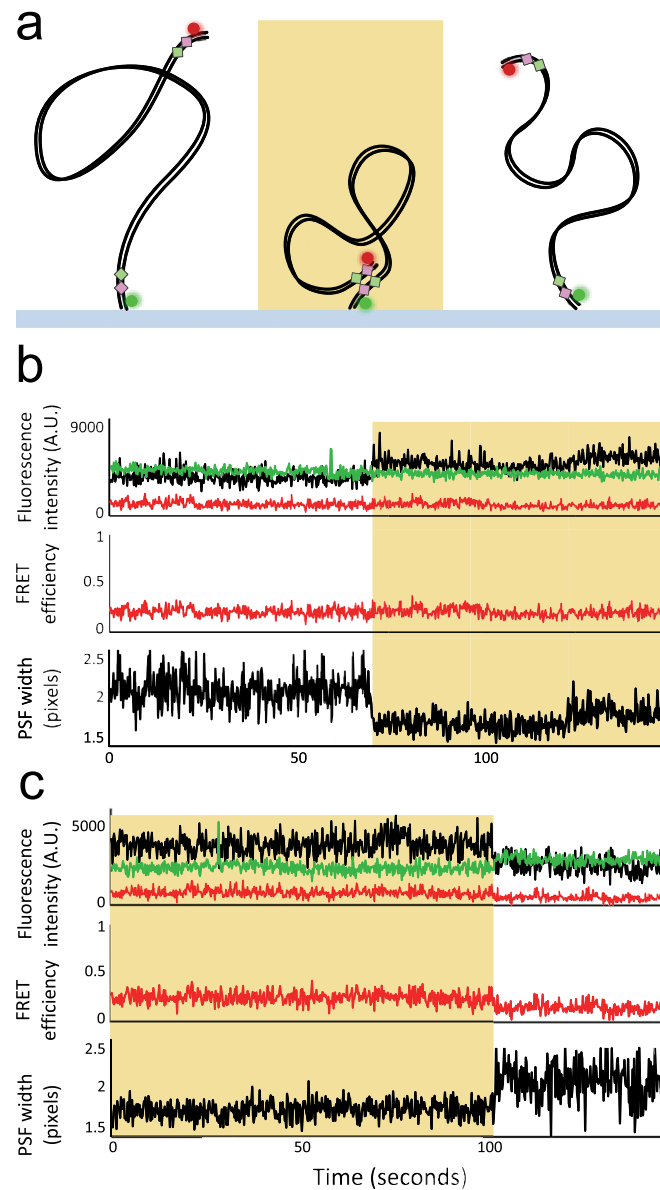


Fig. S7. Using an alternative substrate to assess the stability of the recombinant product complex. (A) Schematic of substrate used with *loxP* sites in an inverted arrangement. BS-S complex formation leads to a decrease in PSF width but no FRET. Recombination results in the inversion of the DNA linking the two *loxP* sites of the substrate, and dissociation of the product complex leads to a return to high PSF. (B) Example time trace of a single substrate molecule undergoing complex formation. (C) Time trace from a separate molecule showing dissociation of a complex to a long DNA, which we attribute to dissociation of the recombinant product synaptic complex.

Table S1. Accurate FRET efficiencies and the corresponding distances from populations fitted to histograms in Fig. 3

Population	Accurate FRET	SD	Distance (Å)	SD
wt, productive	0.58	0.07	67	5
wt, nonproductive (high)	0.65	0.06	64	5
wt, nonproductive (low)	0.42	0.10	75	7
A36V	0.62	0.09	65	6
A312T	0.64	0.07	64	5
K201A	0.44	0.11	74	7

Table S2. Fit parameters of width and SD for the Gaussian fits to histograms in Fig. 3

Population	Mean	SEM	SD of the fit	SEM of the SD
wt, productive	0.36	0.013	0.085	0.006
wt, nonproductive (high)	0.43	0.015	0.065	0.008
wt, nonproductive (low)	0.26	0.023	0.057	0.011
A36V	0.42	0.018	0.067	0.009
A312T	0.42	0.021	0.073	0.011
K201A	0.28	0.009	0.056	0.004